International Journal of Fracture **95:** 19–39, 1999.

The effects of heterogeneity and anisotropy on the size effect in cracked polycrystalline films

R. BALLARINI[1*], R.L. MULLEN[1] and A.H. HEUER[2]
[1]*Department of Civil Engineering, Case Western Reserve University, Cleveland, Ohio 44106-7201, U.S.A.*
[2] *Department of Materials Science and Engineering, Case Western Reserve University, Cleveland, Ohio 44106-7204*

Received 9 June 1998; accepted in revised form 2 December 1998

Abstract. A model is developed for quantifying the size effect due to heterogeneity and anisotropy in polycrystalline films. The Monte Carlo finite element calculations predict the average and standard deviation of the *microscopic* (local) stress intensity factors and energy release rate of a crack in a columnar aggregate of randomly orientated, perfectly bonded, orthotropic crystals (grains) under plane deformation. The boundary of the near-tip region is subjected to displacement boundary conditions associated with a *macroscopic* (far field or nominal) Mode-I stress intensity factor and average elastic constants calculated for the uncracked film with a large number of grains. The average and standard deviation of the microscopic stress intensity factors and energy release rate, normalized with respect to the macroscopic parameters, are presented as functions of the number of grains within the near-tip region, and the parameters that quantify the level of crystalline anisotropy. It is shown that for a given level of anisotropy, as long as the crack tip is surrounded by at least ten grains, then the expected value and standard deviation of the crack tip parameters are insensitive to the number of crystals. For selected values of crystalline anisotropy, the probability distributions of Mode-I stress intensity factor and stress ahead of the crack are also presented. The results suggest that the size effect due to heterogeneity and anisotropy is weak; crack initiation load and direction are governed only by the details of the grains in the immediate vicinity of the crack tip.

Key words: Anisotropy, heterogeneity, polycrystalline.

1. Introduction

In linear elastic fracture mechanics (LEFM) theory of homogeneous materials, the nominal stress σ_n is expressed in terms of the stress intensity factor K_{I} as

$$\sigma_n = \frac{K_{\mathrm{I}}}{a^{1/2}F}, \tag{1}$$

where a is the crack length and F is a dimensionless function which depends on the loading and specimen geometry. In this one parameter system, the critical stress σ_n^c is determined, for the desired loading, geometry, and crack length, by equating the stress intensity factor with the material's fracture toughness $K_{\mathrm{I}c}$. The associated crack stress analysis for the homogeneous material produces a *macroscopic* (nominal or far-field) stress intensity factor, which will henceforth be denoted K_{I}^{∞}. The critical stress intensity factor criterion is equivalent to the condition that the energy release rate, defined for *self-similar* extension as $G_{\mathrm{I}}^{\infty} \equiv (K_{\mathrm{I}}^{\infty})^2/E'$, reaches a critical value $G_{\mathrm{I}c} = K_{\mathrm{I}c}^2/E' = 2\gamma$, where $E' = E$ for plane stress, $E' = E/(1-\nu^2)$

* Correspondence address: Civil Eng. Dept., Case Western Reserve University, Cleveland, OH 44106-7201, U.S.A. e-mail: rxb7@po.cwru.edu

for plane strain, γ is the surface energy, E is Young's modulus, and ν is Poisson's ratio. LEFM is based on the assumption that the 'process zone' in the immediate vicinity of the crack tip, within which irreversible deformation occurs and linear elasticity breaks down, is sufficiently small compared to other relevant length scales, so that there exists an annular region surrounding it within which the stresses are dominated by the elastic stress intensity factor. Moreover, the assumption of homogeneity implicitly assumes that the process zone extends from the crack tip to a distance much larger than the crystal (grain) size, and thus engulfs and in turn is engulfed by a sufficiently large number of grains that behave as a homogeneous medium. Abdel-Tawab and Rodin (1997) suggest that a material's tendency to behave homogeneously can be screened by the grain brittleness GB, defined as

$$GB \equiv \frac{d}{r_p}. \tag{2}$$

Here d is the grain size, and r_p is the size of the process zone, which can be estimated as

$$r_p = 0.1c \left(\frac{K_{\mathrm{I}c}}{\sigma_u} \right)^2, \tag{3}$$

where σ_u represents a limiting stress appropriate for a given material system (yield stress for metals, tensile strength for brittle materials), and c is a constant close to unity. The assumption of homogeneity is appropriate for $GB \ll 1$; if GB is not sufficiently small, then the irreversible deformations at the crack tip do not overwhelm microstructure induced inhomogeneity, and the details of the microstructure surrounding the process zone may have a significant effect on the fracture process. Indeed, because of the randomness of the distribution and orientation of the grains, these effects will be of a statistical nature.

It has been established experimentally that the fracture toughness of most engineering materials depends on specimen dimensions. The amount of this so called 'size effect', which results from differences in the relative size of the process zone in geometrically similar but different sized specimens, varies from material to material. Much research has been conducted by the fracture mechanics community in the past twenty years aimed at describing and predicting the size effect. This effort has produced scaling laws through cohesive zone models (Cox and Marshall, 1994), dimensional analysis (Bazant, 1993) and fractal geometry concepts (Carpinteri, 1994). The main advantage of these formulations is that they can be easily implemented into analysis/design tools for predicting crack propagation in engineered structures. However, by smearing out the details of the deformation mechanisms involved in the fracture process, and by treating the phenomena deterministically and/or phenomenologically, they lose information that can be valuable in the interpretation of scatter in experimental data.

This paper focuses on characterization of the fracture mechanics parameters of a crack in a columnar aggregate of randomly orientated crystals under plane deformation. The following question is addressed: given the parameters that quantify the level of crystalline anisotropy, the number of grains in a unit volume, and a far field loading defined by K_{I}^{∞}, what are the average values and standard deviations of the *microscopic* (local) stress intensity factors K_{I}^{l} and K_{II}^{l} and energy release rate G^{l}? This information, which should shed some light on why the fracture toughness of brittle polycrystalline structures is prone to scatter and size effects, can be obtained only by using micromechanical models that treat the microstructural details and associated deformation mechanisms explicitly (Abdel-Tawab and Rodin, 1997; Ballarini

et al., 1995; Jha et al., 1997; Jha, 1997). As stated in (Abdel-Tawab and Rodin, 1997), the ultimate goal of such models is to develop size effect maps analogous to those (Frost and Ashby, 1982) for deformation mechanisms, and that characterization of the individual size effects produced by inhomogeneity is the first step towards this end. The next logical step towards this end, which is being taken at the present time by the authors, is to include the effects of the microcracking that often develops in the vicinity of the crack tip. Abdel-Tawab and Rodin's analysis (Abdel-Tawab and Rodin, 1997), which addressed issues similar to those discussed in this paper, was developed for characterizing the fracture mechanics of crystalline columnar ice. Their approximate analytical and finite element plane strain models calculate the difference between K_{I}^{∞} and K_{I}^{l} at the tip of a crack surrounded by a *large* number of brittle hexagonal crystals with perfectly bonded interfaces. This local parameter is needed because, for a heterogeneous material, G_{I}^{∞} and γ in the fracture criterion should be replaced by G^{l} and γ^{l}, where γ^{l} is the local value of critical energy release rate. Abdal-Tawab and Rodin's contribution showed that, in an aggregate comprised of a very large number of grains, the grains remote from the crack tip do not induce significant differences between the macroscopic and microscopic stress intensity factors. For example, their calculations showed that even for highly anisotropic crystals, K_{I}^{l} is only twenty percent less than K_{I}^{∞} (K_{II}^{l} was negligible for the nominal mode-I loading). They concluded that for such materials the contribution of inhomogeneity to the size effect is relatively weak. Moreover, their results suggest that the crack tip parameters of materials with large values of GB are controlled by only a few grains near the crack tip, and provide a rational explanation of why fracture toughness data exhibits significant statistical effects. As they pointed out, the results are expected to change dramatically if microcracking within grains or along grain boundaries is included in the models.

One of the issues that was not discussed in (Abdel-Tawab and Rodin, 1997) is fatigue. For brittle polycrystalline materials, crack growth under cyclic K_{I}^{∞}, or under constant K_{I}^{∞} and corrosive environments, has been quantified with power law functions of the type $\mathrm{d}a/\mathrm{d}N = C(\Delta K_{\mathrm{I}}^{\infty})^{m}$ and $\mathrm{d}a/\mathrm{d}t = D(K_{\mathrm{I}}^{\infty})^{p}$, where N and t represent number of cycles and time, respectively, and C, D, m and p are experimentally measured constants. Because m and p are typically larger than, say 10, small heterogeneity induced fluctuations in local crack tip parameters may suddenly become important in lifetime predictions.

The Monte Carlo finite element model presented in this paper extends the calculations presented in (Abdel-Tawab and Rodin, 1997) to include *orthotropic* crystals and an *arbitrary* number of crystals within a unit volume. Furthermore, the model can be generalized to quantify the effects of microcracking in the process zone that often surrounds the crack tip in a brittle system. The model was developed to quantify the effects of heterogeneity and anisotropy on the *scatter* and potential size effects in the *nominal* fracture toughness (critical value of K_{I}^{∞}) and fatigue data of microelectromechanical systems (MEMS), whose dimensions are of the same order as the microstructure. Using a first generation microfracture specimen, they reported (Ballarini et al., 1997) that the critical J integral (which provided a nominal fracture toughness) of notched polycrystalline silicon, which is one of the principal materials currently used in the fabrication of MEMS devices, exhibited significant scatter, but was not sensitive to the number of crystals in the uncracked ligament. The number of crystals in the uncracked ligament was larger than ten. Figure 1(a) shows the second generation microfracture device that is currently being used by the authors to study fatigue and fracture of MEMS. The close-up view of the crack path through the originally uncracked ligament shown in Figure 1(b) clearly demonstrates that the characteristic lengths in MEMS devices are of the same order of magnitude as the grain size. These experiments are ideal for studying statistical effects

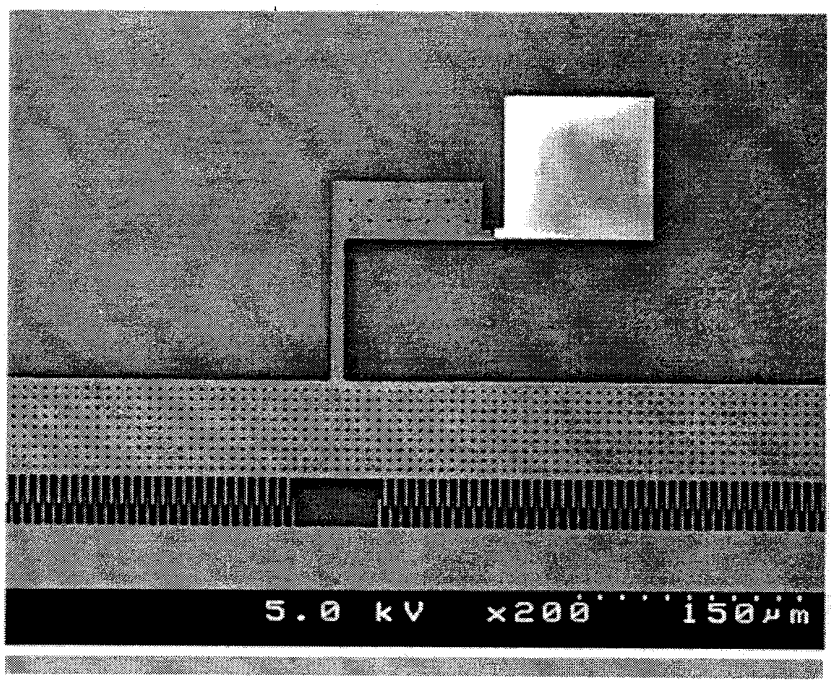

(a)

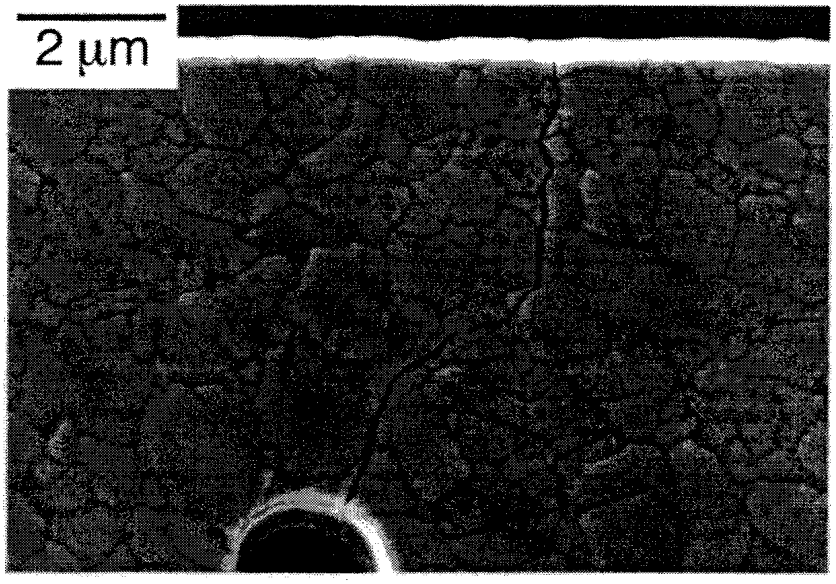

(b)

Figure 1. (a) Polycrystalline silicon microfracture specimen consisting of a cantilevered beam with a reduced section containing an initial smooth notch. The electrostatic load is provided by a comb actuator system, partially shown at the bottom of the figure; (b) Close-up of notch-tip showing the crack propagation path.

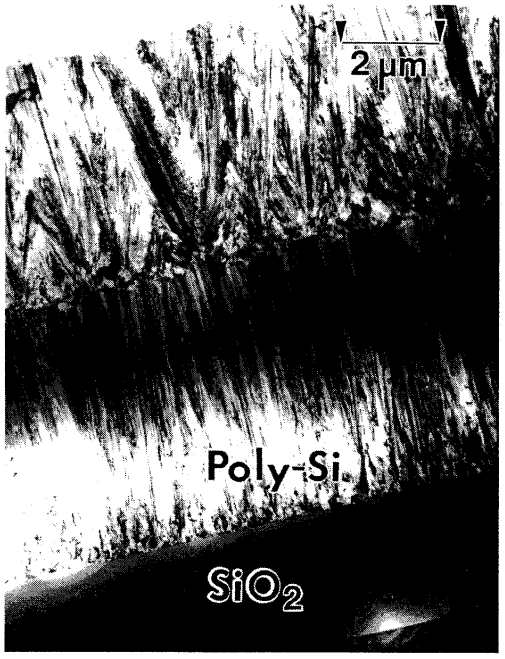

Figure 2. Cross-sectional transmission electron micrograph (TEM) of chemical vapor deposition film. This particular film was deposited using a two-step process, as indicated by the two layers of nearly columnar polysilicon.

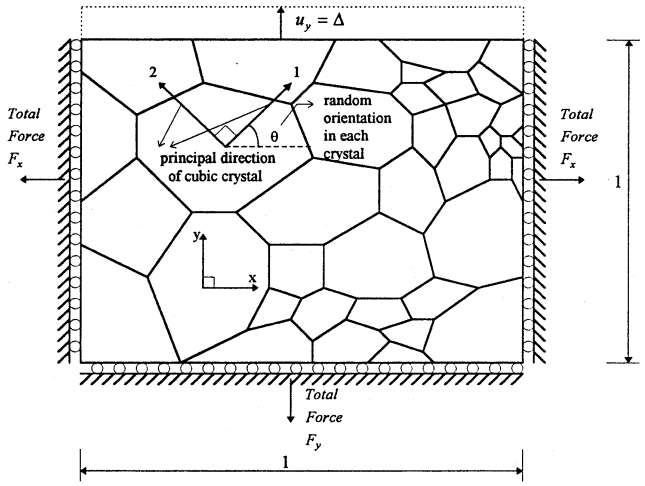

Figure 3. Poisson-Voronoi tessellation of microstructure for n-grains.

in the fracture mechanics of brittle materials; the integrated circuit processing technology used to fabricate the specimen involves batch fabrication, allowing production of a large number of identical specimens that are both dimensionally accurate and inexpensive. The details of the experimental program and results will be presented in a future communication.

Silicon possesses cubic symmetry, a $K_{Ic} \approx 0.8\,\text{MPa}\sqrt{\text{m}}, \sigma_{\text{ult}} = 1.2\,\text{GPa}$, and for the specimens shown in Figure 1, a crystal size $d \approx 0.5\mu\text{m}$. The resulting $GB \approx 10$ suggests that heterogeneity and anisotropy may play a significant role in the fracture behavior of

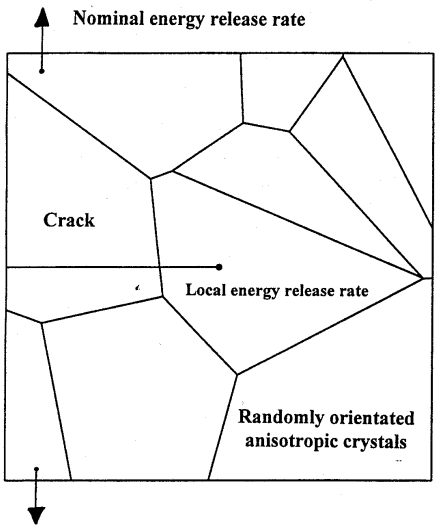

Figure 4. Poisson-Voronoi tessellation of a crack in an aggregate of crystals.

polycrystalline silicon devices that are comprised of a small number of grains (connecting beams are typically a few microns wide, and may be comprised of less than ten grains). As observed in the SEM micrograph in Figure 2, the microstructure of typical devices is (nearly) columnar. This supports the assumption of two dimensional behavior in subsequent finite element analyses. While the film is in plane stress, plane strain was assumed for convenience.

2. Near-tip mechanics

This section defines the mechanics problem and a review of the deterministic *dual length scale mechanics* near the tip of a crack in a polycrystalline material. Before proceeding to the fracture mechanics problem, the procedure for determining the nominal elastic constants of a columnar aggregate of anisotropic crystals is presented. Figure 3 shows the geometry and loading of the model used to calculate the average elastic constants of an aggregate of randomly orientated anisotropic crystals of average size l. Figure 4 shows the same aggregate with a crack, loaded, as explained subsequently, with prescribed displacements at the boundary consistent with a macroscopic stress intensity factor K_{I}^{∞} (or G_{I}^{∞}). The problem consists of calculating the *average* and *standard deviation* of the microscopic crack tip parameters K_{I}^{l}, K_{II}^{l} and G^{l} as functions of the level of crystalline anisotropy and the number of grains in a unit volume. This information is needed because the crack will extend at a critical combination of the microscopic stress intensity factors K_{I}^{l} and K_{II}^{l}, which are linearly related to K_{I}^{∞}, but otherwise depend on the details of the microstructure in the immediate vicinity of the crack tip. Alternatively, the crack can be assumed to propagate at an energy release rate G^{l} (which is defined subsequently) equal to a critical value γ^{l}. The propagation criterion in a single crystal, which is beyond the scope of this paper, is an important issue that is receiving attention (Azhdari and Nemat-Nasser, 1996; 1998). The problem of predicting crack propagation in the polycrystalline medium is complicated by the fact that function F in (1) now depends on details such as the number of crystals in a unit area, the relative position of the crack tip within the crystal, and the orientations of the principal material directions within each crystal.

The crystalline structure in both models is approximated as a Poisson-Voronoi tessellation, consisting of n grains, using the approach taken in (Kumar, 1992; Mullen et al., 1997). Each grain is assumed to possess either cubic or orthotropic symmetry.

With respect to the local coordinate axes 1–2 shown in Figure 3, which represent the principal material directions of a typical grain, the stress-strain relations are given, in matrix and component form, by Hooke's law in plane strain

$$\{\sigma\} \equiv \begin{Bmatrix} \sigma_{11} \\ \sigma_{22} \\ \sigma_{12} \end{Bmatrix} = [S]\{\varepsilon\} \equiv \begin{bmatrix} s_{11} & s_{12} & 0 \\ s_{12} & s_{22} & 0 \\ 0 & 0 & 2s_{44} \end{bmatrix} \begin{Bmatrix} \varepsilon_{11} \\ \varepsilon_{22} \\ \varepsilon_{12} \end{Bmatrix}, \tag{4}$$

where σ_{ij} and ε_{ij} $(i, j = 1, 2)$ are, respectively, components of the symmetric stress and strain tensors. System 1–2 is rotated through angle θ from the global x-axis. The stiffness coefficients in the global x-y axes are calculated using standard transformation formulas. The level of anisotropy is quantified by the parameters A, $\overline{\nu}$ and λ, defined as

$$A \equiv \frac{2s_{44}}{s_{11} - s_{12}}, \tag{5a}$$

$$\overline{\nu} \equiv \frac{s_{12}}{s_{11} + s_{12}}, \tag{5b}$$

$$\lambda = \frac{s_{11}}{s_{22}}. \tag{5c}$$

For isotropic materials $A = 1, \overline{\nu} = \nu$, and $\lambda = 1$. The randomness of the orientation of the principal directions is introduced, in each of m simulations (m varied from 200–300), by assigning, to each cell, a uniformly distributed random angle θ, where $0 < \theta < 2\pi$. The nominal Poisson's ratio and nominal plane strain Young's modulus are defined as $\nu^n \equiv \nu$ and $E^n/(1 - (\nu^n)^2)$, respectively. The normalized plane strain modulus E, is obtained by normalizing the nominal plane strain modulus with respect to the 'isotropic' plane strain modulus $E^{\text{isotropic}}$, which is obtained by equating the first entry in the stiffness matrix S, for $A = 1$ (for fixed $\overline{\nu}$), with that of an isotropic material, i.e. $E^{\text{isotropic}} \equiv c_{11}(1-2\overline{\nu})/(1-\overline{\nu}^2)$. For an aggregate comprised of a very large number of grains (an average of $n = 750$ grains within a unit area of film), Figures 5 show, as functions of A and $\overline{\nu}$, the average values of the nominal Poisson's ratio and normalized plane strain Young's modulus. The most interesting result in these figures is the negative nominal Poisson's ratio that results from crystalline anisotropy, as first reported in (Mullen et al., 1997). As discussed in (Mullen et al., 1997), the nominal elastic constants are more sensitive to $\overline{\nu}$ than to λ.

Figures 6 present, for highly anisotropic cubic and orthotropic crystals, the fraction of occurrences of the average plane strain modulus. It is observed that these are nearly symmetric about the mean, and are associated with a well defined peak.

The near-tip mechanics is summarized through the local-global representation of the cracked polycrystalline plane region shown in Figure 7. Let L represent the macroscopic length scale (crack length, uncracked ligament length, or any other relevant characteristic length), and recall that l represents the average grain size. For a given (deterministic) aggregate, it is expected that for large values of L/l, a near-tip, *small scale heterogeneous* zone exists, and arguments analogous to those presented for small scale process zones can be used to study

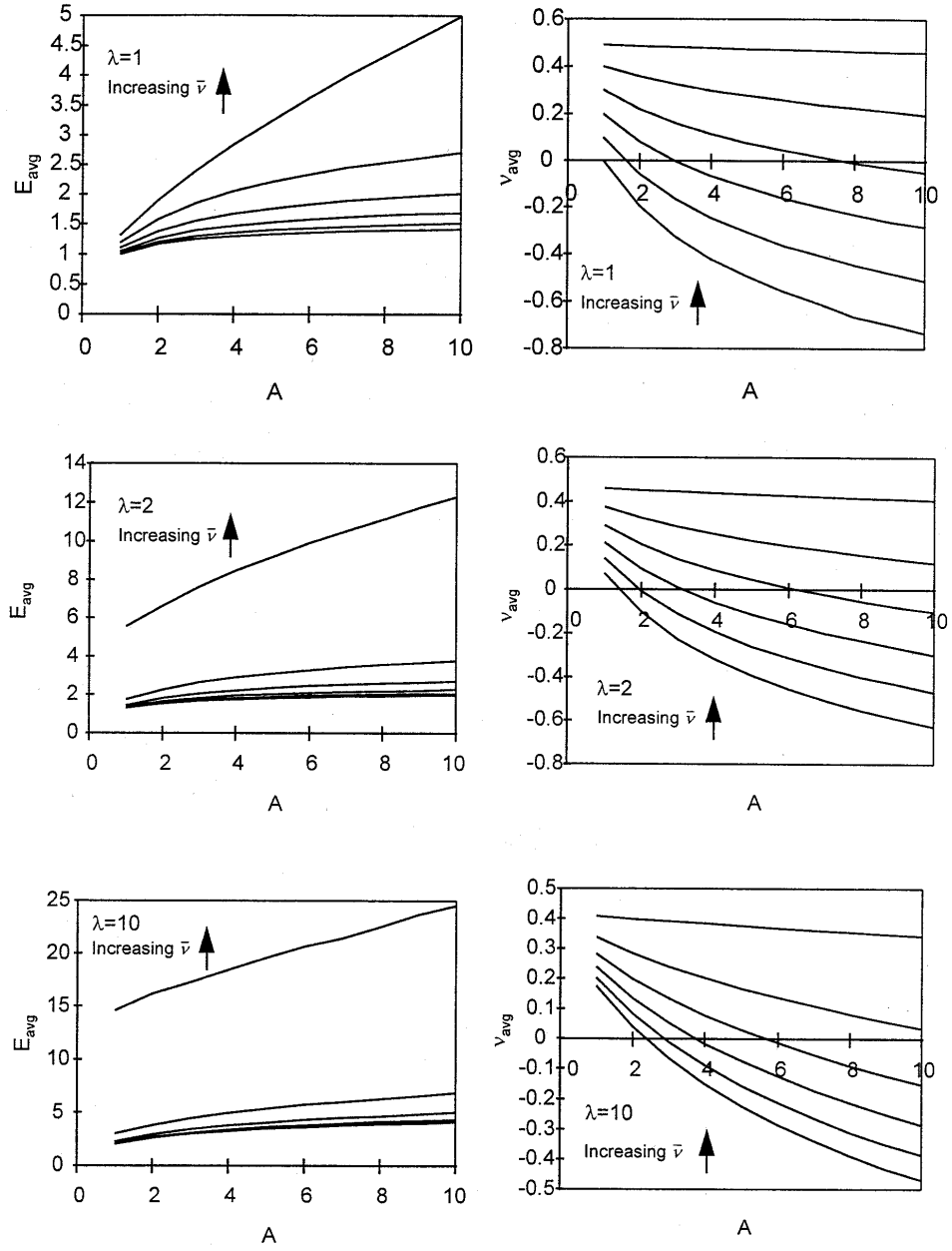

Figure 5. Average values of normalized plane strain Young's modulus and Poisson's ratio as functions of anisotropy parameters; $\overline{\nu} = 0, 0.1, 0.2, 0.3, 0.4, 0.5$.

the evolution of the near-tip stress fields (Ballarini et al., 1995; Jha et al., 1997; Jha, 1977). For example, in small scale yielding, the near-tip plastic zones that develop with increasing load disturb the singular elastic solution giving rise to other near-tip asymptotics such as the HRR fields in deformation plasticity and power law hardening materials (Rice and Rosengren, 1968; Hutchinson, 1968). Similarly, it is expected that for the polycrystalline material, the heterogeneity perturbs the singular fields predicted by the homogeneized aysmptotic solution giving rise to dual asymptotics consistent with the dual length scales in the near-tip region.

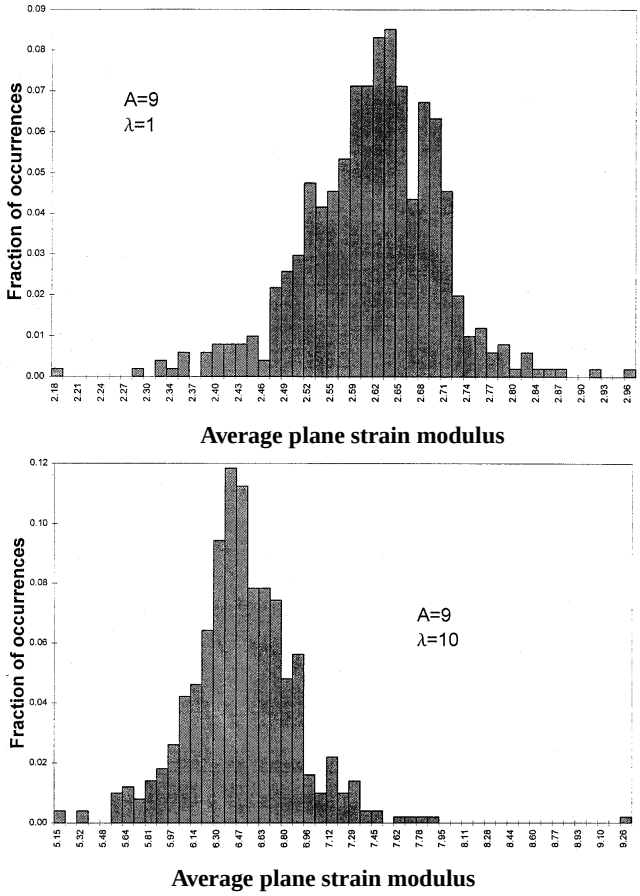

Figure 6. Distributions of average plane strain modulus.

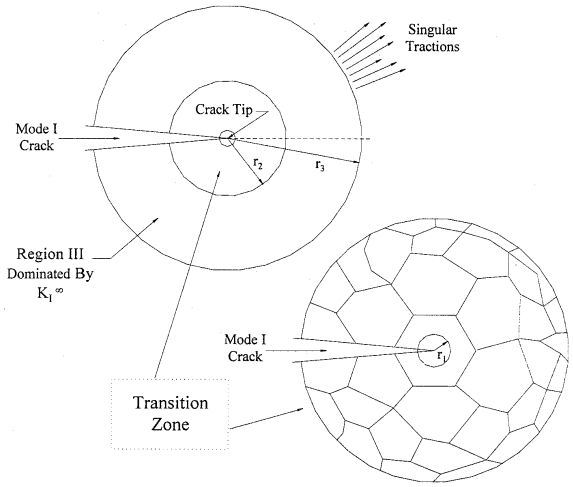

Figure 7. A schematic representation of the regions dominated by distinct asymptotics.

Moreover, for large L/l, the mechanical response of the polycrystalline material at distances sufficiently away from the physical crack tip can be studied by ignoring the microstructure while employing the properties of a homogeneous isotropic medium instead. The latter properties can be calculated using the properties of the individual crystals through homogeneization techniques; this paper uses the results presented in Figures 5. The stresses associated with the response of the homogeneous medium reflect average stress measures acting over the length of an appropriate microstructural unit cell. Under such conditions, the average unit cell stresses and displacements in the neighborhood of the crack tip are square root singular, and can be characterized via an isotropic macroscopic stress intensity factor K_{I}^{∞}. These are given by (Anderson, 1995)

$$\left\{ \begin{array}{c} \sigma_{xx} \\ \sigma_{yy} \\ \sigma_{xy} \end{array} \right\} = \frac{K_{\mathrm{I}}^{\infty}}{\sqrt{2\pi r}} \cos\tfrac{1}{2}\theta \left\{ \begin{array}{l} 1 - \sin\tfrac{1}{2}\theta \sin\tfrac{1}{2}3\theta \\ 1 + \sin\tfrac{1}{2}\theta \sin\tfrac{1}{2}3\theta \\ \sin\tfrac{1}{2}\theta \cos\tfrac{1}{2}3\theta \end{array} \right\}, \tag{6}$$

$$\left\{ \begin{array}{c} u_x \\ u_y \end{array} \right\} = \frac{K_{\mathrm{I}}^{\infty}}{2G} \sqrt{\frac{r}{2\pi}} \left\{ \begin{array}{l} \cos\tfrac{1}{2}\theta \left[\kappa - 1 + 2\sin^2\tfrac{1}{2}\theta\right] \\ \sin\tfrac{1}{2}\theta \left[\kappa + 1 - 2\cos^2\tfrac{1}{2}\theta\right] \end{array} \right\}, \tag{7}$$

where the r-θ polar coordinate is centered at the crack tip, $G = E/2(1+\nu)$ is the shear modulus, $\kappa = 3 - 4\nu$ for plane strain, $\kappa = (3-\nu)/(1+\nu)$ for plane stress.

As shown in Figure 7, the outermost radius r_3 from the physical crack tip of the zone dominated by K_{I}^{∞} is expected to depend on the macroscopic characteristic length L, and in turn, r_3 is some fraction of L. Thus, in a homogeneized medium, region III as shown in Figure 7 is defined as being dominated by the isotropic singular stress field given by (6) and (7). While this may be a realistic approximation for material systems with large L/l ratios, it is underscored that this approach may only provide useful stress field approximations at material points located within region III at distances from the physical crack tip which are much larger than the microstructural characteristic length l. As a result of the microstructure, it is clear that distinctly different asymptotics will dominate the mechanics at material points in region I (which contains the physical crack tip and extends to a distance r_1), and that these will determine the crack propagation load and direction. The extent r_1 of region I from the crack tip depends on the position of the crack tip relative to the adjacent crystal, and the degree of crystalline anisotropy. The distinct asymptotics dominating regions I and III discussed above are assumed to develop in heterogeneous systems with large L/l. In polycrystalline systems with nearly isotropic crystals, the dominance of region I would clearly prevail over region III, with r_1 extending to r_3. For high levels of anisotropy, the asymptotic fields in regions I and III are expected to be matched through other fields dominating the transition region II, extending from r_1 to r_2.

In the immediate vicinity of the crack tip (region I), which is anisotropic, the stress and displacement components are given by (Sih et al., 1965)

$$\left\{ \begin{array}{c} \sigma_{xx} \\ \sigma_{yy} \\ \sigma_{xy} \end{array} \right\} = \frac{K_{\mathrm{I}}^{l}}{\sqrt{2\pi r}} \mathrm{Re} \left\{ \begin{array}{l} \frac{\mu_1\mu_2}{\mu_1-\mu_2}\left[\frac{\mu_2}{\sqrt{\cos\theta+\mu_2\sin\theta}} - \frac{\mu_1}{\sqrt{\cos\theta+\mu_1\sin\theta}}\right] \\ \frac{1}{\mu_1-\mu_2}\left[\frac{\mu_1}{\sqrt{\cos\theta+\mu_2\sin\theta}} - \frac{\mu_2}{\sqrt{\cos\theta+\mu_1\sin\theta}}\right] \\ \frac{\mu_1\mu_2}{\mu_1-\mu_2}\left[\frac{1}{\sqrt{\cos\theta+\mu_1\sin\theta}} - \frac{1}{\sqrt{\cos\theta+\mu_2\sin\theta}}\right] \end{array} \right\}$$

$$+\frac{K_{\mathrm{II}}^{l}}{\sqrt{2\pi r}}\,\mathrm{Re}\left\{\begin{array}{l}\frac{1}{\mu_1-\mu_2}\left[\frac{\mu_2^2}{\sqrt{\cos\theta+\mu_2\sin\theta}}-\frac{\mu_1^2}{\sqrt{\cos\theta+\mu_1\sin\theta}}\right]\\ \frac{1}{\mu_1-\mu_2}\left[\frac{1}{\sqrt{\cos\theta+\mu_2\sin\theta}}-\frac{1}{\sqrt{\cos\theta+\mu_1\sin\theta}}\right]\\ \frac{1}{\mu_1-\mu_2}\left[\frac{\mu_1}{\sqrt{\cos\theta+\mu_1\sin\theta}}-\frac{\mu_2}{\sqrt{\cos\theta+\mu_2\sin\theta}}\right]\end{array}\right\}, \tag{8a}$$

$$\left\{\begin{array}{l}u_x\\ u_y\end{array}\right\} = K_{\mathrm{I}}^{l}\sqrt{\frac{r}{2\pi}}\,\mathrm{Re}\left\{\begin{array}{l}\frac{1}{\mu_1-\mu_2}[\mu_1 p_2(\cos\theta+\mu_2\sin\theta)^{1/2}-\mu_2 p_1(\cos\theta+\mu_1\sin\theta)^{1/2}]\\ \frac{1}{\mu_1-\mu_2}[\mu_1 q_2(\cos\theta+\mu_2\sin\theta)^{1/2}-\mu_2 q_1(\cos\theta+\mu_1\sin\theta)^{1/2}]\end{array}\right\}$$

$$+K_{\mathrm{II}}^{l}\sqrt{\frac{r}{2\pi}}\,\mathrm{Re}\left\{\begin{array}{l}\frac{1}{\mu_1-\mu_2}[p_2(\cos\theta+\mu_2\sin\theta)^{1/2}-p_1(\cos\theta+\mu_1\sin\theta)^{1/2}]\\ \frac{1}{\mu_1-\mu_2}[q_2(\cos\theta+\mu_2\sin\theta)^{1/2}-q_1(\cos\theta+\mu_1\sin\theta)^{1/2}]\end{array}\right\}, \tag{8b}$$

where Re(Im) denotes real (imaginary) part

$$p_j = c'_{11}\mu_j^2 + c'_{12} - c'_{16}\mu_j, \quad j = 1, 2, \tag{9a}$$

$$q_j = c'_{12}\mu_j + \frac{c'_{22}}{\mu_j} - c'_{26}, \tag{9b}$$

the c'_{ij} are the flexibility coefficients (the components of the inverse of matrix C in (4)), transformed to the global axes, and μ_j are the roots (with positive imaginary parts) of the characteristic equation

$$c'_{11}\mu^4 - 2c'_{16}\mu^3 + (2c'_{12} + c'_{44})\mu^2 - 2c'_{26}\mu + c'_{22} = 0. \tag{10}$$

The energy release rate for self-similar extension is given as

$$G^l = -\tfrac{1}{2}K_{\mathrm{I}}^{l}c'_{22}\,\mathrm{Im}\left[\frac{K_{\mathrm{I}}^{l}(\mu_1+\mu_2)+K_{\mathrm{II}}^{l}}{\mu_1\mu_2}\right] + \tfrac{1}{2}K_{\mathrm{II}}^{l}c_{11}\,\mathrm{Im}[K_{\mathrm{II}}^{l}(\mu_1+\mu_2)+K_{\mathrm{I}}^{l}\mu_1\mu_2]. \tag{11}$$

Because the crystals in a real material are randomly orientated, the behavior of the stress intensity factors and of the stresses in the vicinity of the crack is more complicated; these physical parameters can only be discussed in terms of their probability distributions. Indeed, the scatter in the stresses ahead of the crack may be large enough to render the previous near-tip discussion irrelevant. In other words, distinct asymptotics may not be observed, as will be subsequently shown.

3. Near-tip finite element model

Consider the near-tip plane strain region shown in Figure 4. The physical dimensions of this zone are RxR (with $R = 1$) such that $R \leqslant r_3$, where r_3 signifies the boundary of region III consistent with Figure 7. In this model, the Poisson-Voronoi tessellation approximation of the polycrystalline structure is retained. The region under consideration includes the crack tip, whose position within the crystal is a random variable. The crack surfaces are traction-free. Mode-I loading is applied by prescribing, along the boundary of the region, the displacements in (7). It should be understood that this model does not incorporate finite geometry

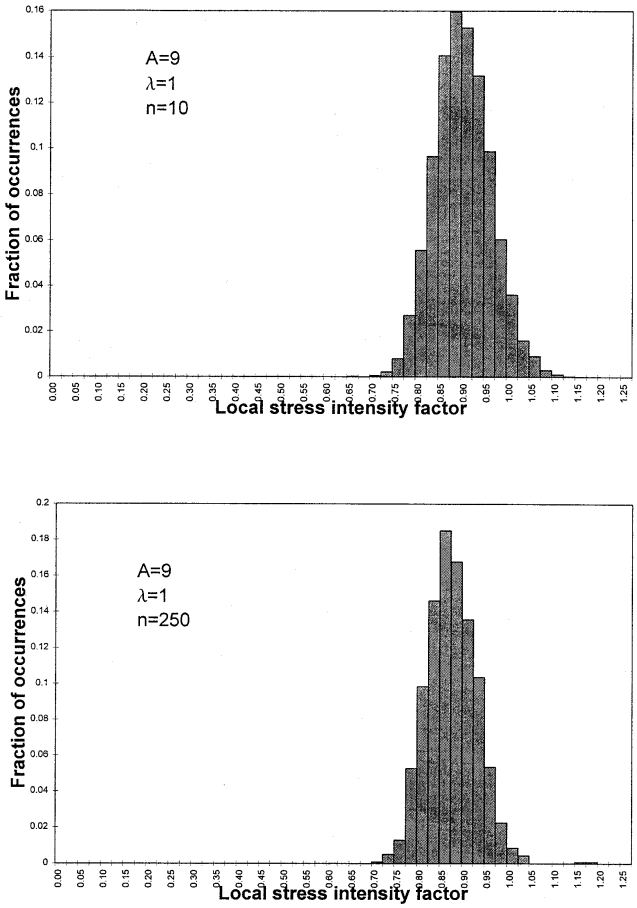

Figure 8. Fraction of occurrences of local stress intensity factor for highly anisotropic cubic crystals.

characteristics. In other words, R does not directly represent a macroscopic length, rather it provides an indirect measure of a macroscopic characteristic length. The only requirement on R is that stated earlier, i.e. $R \leqslant r_3$. Various morphologies corresponding to different L/l are modeled by changing the number of crystals n within the modeled region. It is expected that this approach will capture the various near-tip asymptotics and the transitional characteristics from region I to region III through region II. The relation between R and L could be quantified only by modeling specific finite geometries.

The microscopic stress intensity factors are calculated using the displacement correlation technique (Barsoum, 1977; Ingraffea and Manu, 1980), which involves equating the square root portion of the finite element displacement interpolation of the crack opening and crack sliding displacements, with the analytical values given by (8b). These in turn are used to calculate the local energy release rate.

4. Results

The average and standard deviation (denoted by subscripts avg and sd, respectively) of $K \equiv K_{\mathrm{I}}^{l}/K_{\mathrm{I}}^{\infty}$ and $G \equiv G^{l}/G_{\mathrm{I}}^{\infty}$ are summarized in Table 1. For m simulations (the results presented

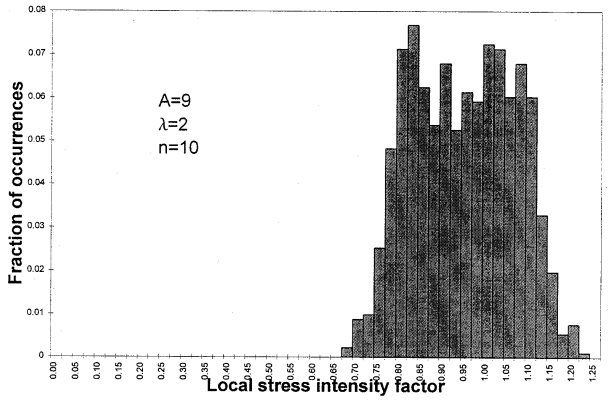

Figure 9. Fraction of occurrences of local stress intensity factor for highly anisotropic, slightly orthotropic crystals.

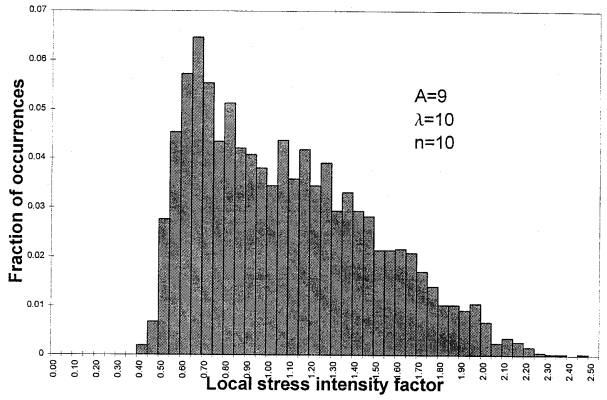

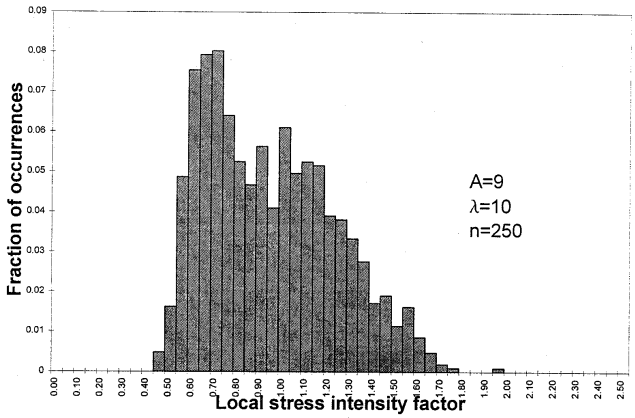

Figure 10. Fraction of occurrences of local stress intensity factor for highly anisotropic orthotropic crystals.

in Table 1 correspond to $m = 200$–400), the standard deviation of x is defined as $\sqrt{(\Sigma_m x^2/(m-1)) - m x_{\text{avg}}^2/(m-1)}$. The results for the isotropic crystals ($A = \lambda = 1$) show that the errors in the calculated stress intensity factors and energy release rates are on the order of a few percent.

Table 1. Calculated crack tip parameters

A	$\overline{\nu}$	λ	n	K_{avg}	G_{avg}	K_{sd}	G_{sd}
1	0	1	10	0.9846	0.9696	0.00692	0.01398
1	0	1	100	0.9848	0.9699	0.00664	0.01377
1	0	1	250	0.9831	0.9666	0.00405	0.0077
1	0	1	500	0.9839	0.968	7.4E-05	0.00015
1	0	2	10	0.9969	0.9818	0.11	0.1203
1	0	2	100	0.9792	0.9575	0.08638	0.08356
1	0	2	250	0.9938	0.9651	0.083	0.07982
1	0	2	500	0.9852	0.9566	0.08823	0.08569
1	0	10	10	1.035	0.9767	0.3407	0.4097
1	0	10	100	0.992	0.8872	0.2745	0.2537
1	0	10	250	0.9601	0.8665	0.2644	0.2299
1	0	10	500	0.9303	0.8395	0.2191	0.1949
1	0.2	2	10	0.9853	0.9647	0.1117	0.1224
1	0.2	2	100	0.9778	0.9574	0.08969	0.09426
1	0.2	2	250	0.9835	0.96	0.09177	0.08819
1	0.2	2	500	0.9771	0.948	0.08347	0.08796
1	0.2	10	10	1.022	0.9687	0.3543	0.4279
1	0.2	10	100	0.9242	0.8389	0.2285	0.2121
1	0.2	10	250	0.9484	0.8393	0.2372	0.2289
1	0.2	10	500	0.9043	0.802	0.2329	0.1912
1	0.4	2	10	0.9558	0.9216	0.1005	0.1155
1	0.4	2	100	0.9485	0.9153	0.08509	0.09749
1	0.4	2	250	0.9417	0.9011	0.0798	0.08157
1	0.4	2	500	0.9489	0.9047	0.08087	0.07973
1	0.4	10	10	0.8912	0.8295	0.2974	0.3599
1	0.4	10	100	0.7999	0.6814	0.1737	0.1962
1	0.4	10	250	0.8087	0.6948	0.1591	0.1861
1	0.4	10	500	0.821	0.7024	0.16	0.1941
3	0	1	10	0.9727	0.9617	0.02514	0.04963
3	0	1	100	0.968	0.9521	0.0216	0.04259
3	0	1	250	0.968	0.9519	0.01872	0.03676
3	0	1	500	0.9675	0.951	0.01883	0.03715
3	0	2	10	0.9855	0.9766	0.1248	0.1485
3	0	2	100	0.978	0.9529	0.105	0.1255
3	0	2	250	0.9705	0.9406	0.1081	0.1212
3	0	2	500	0.966	0.9424	0.1034	0.1123
3	0	10	10	1.061	1.005	0.3984	0.4662
3	0	10	100	0.9493	0.8667	0.2769	0.2766
3	0	10	250	0.9744	0.8869	0.272	0.264
3	0	10	500	0.9866	0.8936	0.2886	0.2839
3	0.2	1	10	0.9732	0.9681	0.02889	0.05746
3	0.2	1	100	0.9729	0.9615	0.1134	0.1235
3	0.2	1	250	0.965	0.9515	0.02521	0.04959

Table 1. (Contd.). Calculated crack tip parameters

A	$\overline{\nu}$	λ	n	K_{avg}	G_{avg}	K_{sd}	G_{sd}
3	0.2	1	500	0.9631	0.9478	0.0253	0.04997
3	0.2	2	10	0.9922	0.9742	0.1181	0.1344
3	0.2	2	100	0.9708	0.9498	0.09824	0.1031
3	0.2	2	250	0.9827	0.9554	0.09156	0.09461
3	0.2	2	500	0.9822	0.9566	0.09097	0.09325
3	0.2	10	10	1.073	1.02	0.3866	0.4397
3	0.2	10	100	1.007	0.9227	0.2873	0.3059
3	0.2	10	250	0.9962	0.9105	0.2977	0.283
3	0.2	10	500	0.9834	0.9068	0.2634	0.2585
3	0.4	1	10	0.9597	0.9542	0.06316	0.118
3	0.4	1	100	0.9431	0.9221	0.05847	0.1119
3	0.4	1	250	0.9481	0.9313	0.05737	0.1074
3	0.4	1	500	0.9577	0.9498	0.0766	0.1456
3	0.4	2	10	0.9774	0.9557	0.1104	0.1238
3	0.4	2	100	0.9764	0.9425	0.09122	0.101
3	0.4	2	250	0.9766	0.9468	0.08848	0.09471
3	0.4	2	500	0.9688	0.9418	0.08373	0.08225
3	0.4	10	10	1.037	0.9866	0.3548	0.3915
3	0.4	10	100	0.9849	0.8779	0.2811	0.2693
3	0.4	10	250	0.9347	0.8322	0.245	0.211
3	0.4	10	500	0.9376	0.8399	0.2447	0.2211
5	0	1	10	0.9711	0.9648	0.04471	0.07122
5	0	1	100	0.9567	0.9364	0.03651	0.05684
5	0	1	250	0.9592	0.9412	0.03872	0.05649
5	0	1	500	0.9604	0.9398	0.04123	0.05033
5	0	2	10	0.9809	0.9708	0.122	0.1472
5	0	2	100	0.9621	0.9425	0.1037	0.119
5	0	2	250	0.9638	0.9488	0.1051	0.1296
5	0	2	500	0.95	0.932	0.09389	0.1007
5	0	10	10	1.055	1.022	0.4035	0.4877
5	0	10	100	0.9945	0.9171	0.3043	0.3055
5	0	10	250	0.9684	0.9034	0.2968	0.3025
5	0	10	500	0.9475	0.8725	0.2836	0.2766
5	0.2	1	10	0.9593	0.9577	0.03936	0.07897
5	0.2	1	100	0.9506	0.9396	0.0345	0.06848
5	0.2	1	250	0.9524	0.9431	0.03362	0.06683
5	0.2	1	500	0.952	0.9325	0.1455	0.1505
5	0.2	2	10	0.9759	0.9687	0.1191	0.1415
5	0.2	2	100	0.9581	0.9437	0.1003	0.1194
5	0.2	2	250	0.9723	0.9534	0.09271	0.1078
5	0.2	2	500	0.9712	0.9447	0.08757	0.101
5	0.2	10	10	1.077	1.063	0.4268	0.5295
5	0.2	10	100	0.9624	0.8901	0.2908	0.3069

Table 1. (Contd.). Calculated crack tip parameters

A	$\overline{\nu}$	λ	n	K_{avg}	G_{avg}	K_{sd}	G_{sd}
5	0.2	10	250	0.9841	0.892	0.286	0.27
5	0.2	10	500	0.9676	0.8927	0.2917	0.2902
5	0.4	1	10	0.9303	0.9299	0.04891	0.09878
5	0.4	1	100	0.9123	0.8944	0.05005	0.09767
5	0.4	1	250	0.9143	0.8976	0.04615	0.09006
5	0.4	1	500	0.9229	0.9153	0.05063	0.1015
5	0.4	2	10	0.9762	0.9643	0.1165	0.1416
5	0.4	2	100	0.9662	0.9458	0.09975	0.1183
5	0.4	2	250	0.9558	0.9297	0.09285	0.1054
5	0.4	2	500	0.9677	0.9406	0.09325	0.1083
5	0.4	10	10	1.105	1.054	0.3949	0.466
5	0.4	10	100	0.9975	0.8837	0.2743	0.2613
5	0.4	10	250	0.9845	0.8991	0.2702	0.2659
5	0.4	10	500	0.9684	0.8628	0.2486	0.2308
9	0	1	10	0.9579	0.956	0.04177	0.08366
9	0	1	100	0.9386	0.9162	0.02891	0.0563
9	0	1	250	0.9372	0.9134	0.02816	0.05491
9	0	1	500	0.9444	0.9254	0.04802	0.07167
9	0	2	10	0.9678	0.9596	0.1291	0.1637
9	0	2	100	0.9439	0.922	0.1051	0.1243
9	0	2	250	0.9269	0.9031	0.09488	0.1116
9	0	2	500	0.9367	0.9143	0.09702	0.1162
9	0	10	10	1.038	1.041	0.4261	0.5412
9	0	10	100	0.9199	0.8478	0.3257	0.3755
9	0	10	250	0.9021	0.8214	0.2705	0.2901
9	0	10	500	0.9342	0.8535	0.3035	0.3358
9	0.2	1	10	0.94	0.948	0.04818	0.09767
9	0.2	1	100	0.9255	0.9172	0.04194	0.08291
9	0.2	1	250	0.9188	0.9035	0.03489	0.06888
9	0.2	1	500	0.9227	0.9111	0.03523	0.06972
9	0.2	2	10	0.9676	0.9695	0.1692	0.2056
9	0.2	2	100	0.9378	0.9171	0.0987	0.123
9	0.2	2	250	0.935	0.9131	0.1016	0.1204
9	0.2	2	500	0.9463	0.9269	0.09811	0.1199
9	0.2	10	10	1.073	1.073	0.4394	0.5444
9	0.2	10	100	0.9414	0.866	0.3021	0.31
9	0.2	10	250	0.9385	0.8598	0.2882	0.3136
9	0.2	10	500	0.921	0.8624	0.305	0.3383
9	0.4	1	10	0.9006	0.9132	0.05919	0.1214
9	0.4	1	100	0.8835	0.8786	0.06104	0.1216
9	0.4	1	250	0.875	0.8609	0.054	0.1073
9	0.4	1	500	0.869	0.8504	0.06049	0.1189
9	0.4	2	10	0.963	0.9636	0.127	0.1614

Table 1. (Contd.). Calculated crack tip parameters

A	$\overline{\nu}$	λ	n	K_{avg}	G_{avg}	K_{sd}	G_{sd}
9	0.4	2	100	0.9376	0.9131	0.1017	0.1272
9	0.4	2	250	0.9387	0.9093	0.09749	0.1212
9	0.4	2	500	0.9396	0.9168	0.09734	0.1183
9	0.4	10	10	1.089	1.064	0.3915	0.4936
9	0.4	10	100	0.9735	0.9041	0.3105	0.318
9	0.4	10	250	1.009	0.9125	0.2921	0.304
9	0.4	10	500	0.9823	0.8908	0.2944	0.3047

For cubic crystals ($\lambda = 1$), the effects of anisotropy and heterogeneity on the crack tip parameters are relatively small. Consider the results for $n = 500$; for the highest levels of anisotropy considered ($A = 9, \overline{\nu} = 0.4$), the average stress intensity factor is slightly reduced to $\approx 0.87 \pm 0.06$ ($\pm x$ represents $\pm$ one standard deviation), and the average energy release rate is reduced to $\approx 0.85 \pm 0.12$. Moreover, the results are not sensitive to n. Polycrystalline silicon is defined by $A = 1.65, \overline{\nu} = 0.282$; for all values of n, the average stress intensity factor is $\approx 0.93 \pm 0.02$, and the average energy release rate is $\approx 0.91 \pm 0.03$.

The results for orthotropic crystals show that anisotropy and heterogeneity produce significant effects for highly anisotropic crystals. For example, if $n = 500$, $A = 9$, $\lambda = 10$, and $\overline{\nu} = 0.4$, the stress intensity factor is $\approx 0.98 \pm 0.29$, and the energy release rate is $\approx 0.89 \pm 0.30$. Moreover, for highly anisotropic crystals, the results are significantly influenced by the number of grains; for $n = 10$, the standard deviations of the stress intensity factor and energy release rate, for the previous example, increase to 0.39 and 0.49, respectively.

Figures 8–10 show, respectively, the fraction of occurrences of the local Mode-I stress intensity factor for highly anisotropic cubic crystals, highly anisotropic 'slightly' orthotropic crystals, and high anisotropic orthotropic crystals. It is observed that for cubic crystals, the distribution is relatively narrow and nearly symmetric about the mean, while for orthotropic crystals the distribution is wider and not symmetric. Moreover, for orthotropic crystals, a small population of realizations is associated with stress intensity factors that are more than double of the nominal. It is interesting to note that unsymmetric distributions of stress intensity factors were also predicted by the model developed by Scavia and Carpinteri (1991) in their study of the interaction between a crack with a random distribution of surrounding microcracks. However, while Figure 10 indicates peaks in the shielding range and a long tail in the amplification range, similar plots in (Scavia and Carpinteri, 1991) show that distributed microcracking leads to peaks in the amplification range and a long tail in the shielding range.

The scatter of the normalized stress $\sigma \equiv \sqrt{2\pi R}\sigma_{yy}/K_{\text{I}}^{\infty}$ ahead of the crack for highly anisotropic cubic crystals, and highly anisotropic orthotropic crystals, are shown in Figures 11 and 12, respectively. In these figures the distance from the crack tip r, actually represents the nondimensional distance r/R, with $R = 1$. It is observed that for cubic and orthotropic crystals, even at high levels of anisotropy, the dual length scale asymptotics disappear within the scatter; the stress is square root singular, with upper and lower bounds modulated by the deviation of the local stress intensity factor from the mean. Furthermore, the distribution of stress is nearly independent of the number of crystals n.

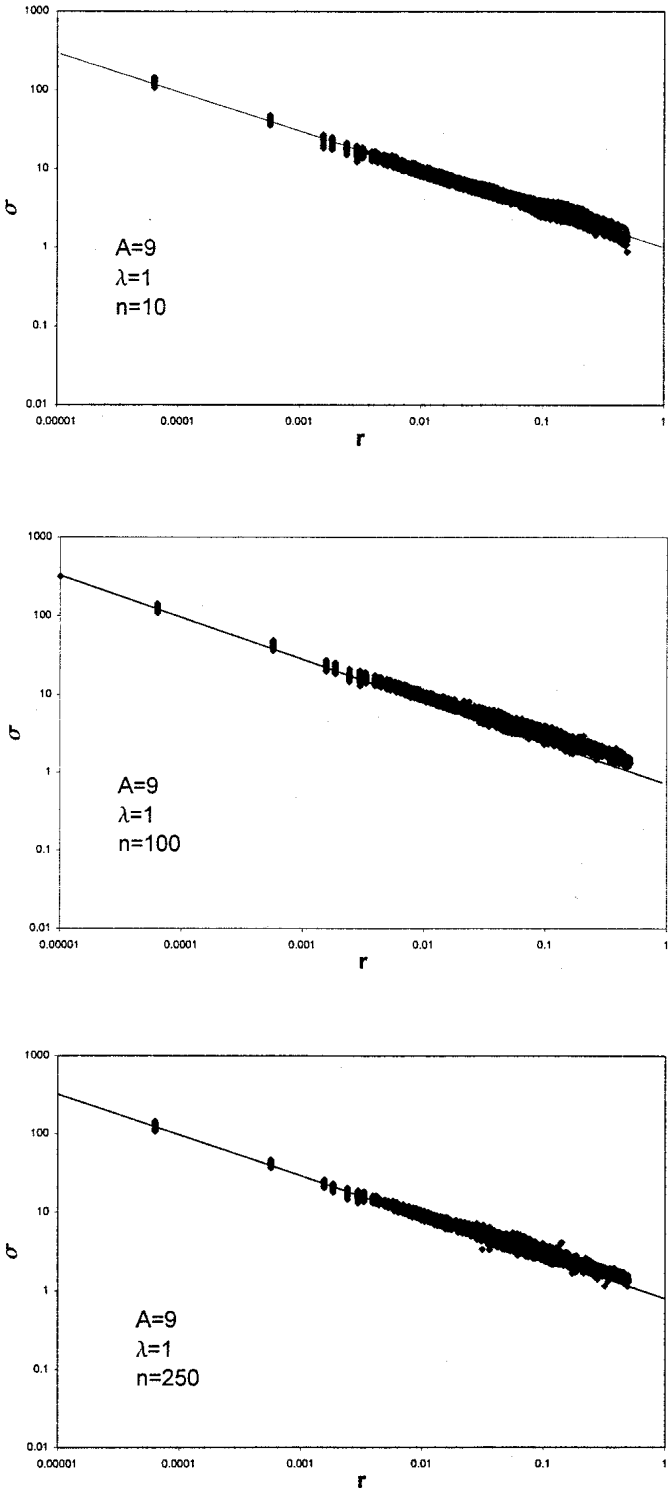

Figure 11. Scatter of normalized stress ahead of crack for several values of $n(\lambda = 1,\ A = 9, \overline{\nu} = 0.4)$.

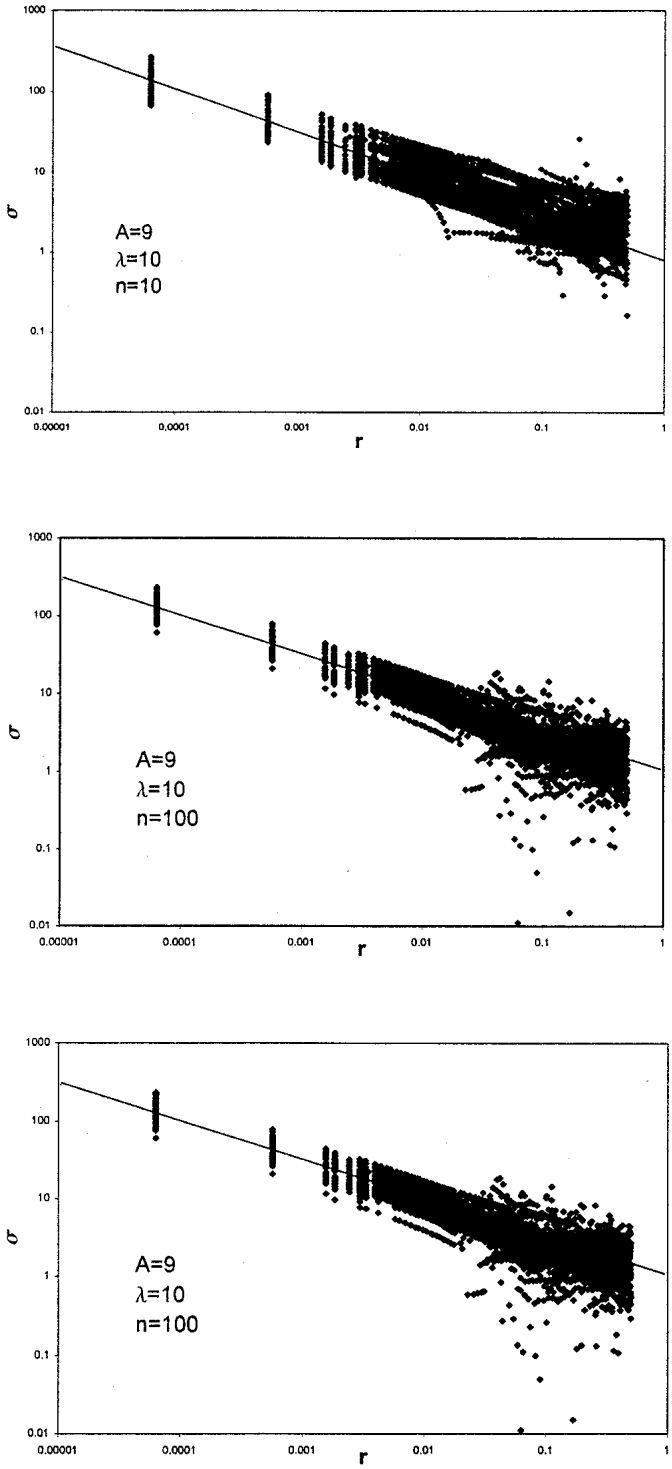

Figure 12. Scatter of normalized stress ahead of crack for several values of $n(\lambda = 10,\ A = 9, \overline{\nu} = 0.4)$.

It is important to note that the effects of anisotropy are expected to increase drastically if cracking within crystals or along grain boundaries is taken into account. The authors are currently calculating these effects, and those of finite geometry.

5. Conclusions

In a columnar aggregate of randomly orientated, perfectly bonded, orthotropic crystals under plane deformation, only the grains surrounding the crack tip significantly perturb the average values and standard deviations of the stress intensity factors and energy release rate from the nominal applied values. For very high levels of crystalline anisotropy, the average values and standard deviations for cubic and orthotropic crystals are perturbed by approximately 10 percent and 30–40 percent, respectively.

Appendix. Calculation of nominal elastic constants

With respect to the global coordinate system x-y-z shown in Figure 3, the film is analyzed under plane strain conditions, $u_z = \partial(\,)/\partial z = 0$, where u_z is the displacement in the z direction, and ( ) denotes any physical quantity. For a given number of grains n, the topology of the microstructure within the *unit* volume shown in Figure 3 is approximated, for *each* of m simulations, as a Voronoi tessellation. The tessellation is constructed by first generating, using a Poisson process, a set of random nucleus points $\boldsymbol{r}_i$ $(i = 1, n)$. The set of all points which are closer to $\boldsymbol{r}_i$ than to any other nucleus $\boldsymbol{r}_j$ $(i \neq j)$ comprise the ith Voronoi cell. The assembly of the n convex, planar edged cells, defines the tessellation. Each grain is discretized with a sufficient number of quadratic displacement finite elements.

For determination of the effective elastic constants, the film *structure* is loaded, as shown in Figure 3, through the following boundary conditions

$$u_y = \Delta, \quad y = 1, \tag{A1}$$

$$u_x = \sigma_{xy} = 0, \quad x = 0, \quad x = 1, \tag{A2}$$

$$u_y = \sigma_{xy} = 0, \quad y = 0. \tag{A3}$$

These are associated with nominal (average) strain components $\varepsilon^n_{yy} = \Delta/1$, $\varepsilon^n_{xx} = 0$, $\varepsilon^n_{xy} = 0$. The finite element method is used to calculate the total reaction forces (per unit thickness) F_x and F_y shown in Figure 3, which for the unit length edges, correspond to nominal stress components σ^n_{xx} and σ^n_{yy}, respectively. The associated nominal values of the Poisson ratio ν^n and plane strain Young's modulus $\overline{E}^n \equiv E^n/[1-(\nu^n)^2]$ are defined by invoking Hooke's law for the *isotropic* continuum under plane strain conditions

$$\begin{Bmatrix} \sigma^n_{xx} = F_x \\ \sigma^n_{yy} = F_y \\ \sigma^n_{xy} = 0 \end{Bmatrix} = \frac{E^n}{(1+\nu^n)(1-2\nu^n)} \begin{bmatrix} 1-\nu^n & \nu^n & 0 \\ \nu^n & 1-\nu^n & 0 \\ 0 & 0 & (1-2\nu^n) \end{bmatrix} \begin{Bmatrix} \varepsilon^n_{xx} = 0 \\ \varepsilon^n_{yy} = \Delta \\ \varepsilon^n_{xy} = 0 \end{Bmatrix}. \tag{A4}$$

Equations (A4) provide

$$\nu^n = \frac{1}{1+\frac{F_y}{F_x}}, \tag{A5}$$

$$\overline{E}^n = \frac{E^n}{[1-(\nu^n)^2]} = \frac{(1+\nu^n)(1-2\nu^n)}{\nu^n[1-(\nu^n)^2]}\frac{F_x}{\Delta}. \tag{A6}$$

The steps described above are repeated m times for each value of n.

$\overline{E}^n$ is normalized with the 'isotropic' plane strain Young's modulus $\overline{E}^{\text{isotropic}}$ obtained by equating the first entry in the stiffness matrix for cubic symmetry, for $A = 1$ (for fixed $\overline{\nu}$) with that of an isotropic material, i.e.

$$\overline{E}^{\text{isotropic}} \equiv \frac{c_{11}(1-2\overline{\nu})}{(1-\overline{\nu})^2}. \tag{A6}$$

Acknowledgements

This research was funded by the National Science Foundation under Grants MSS94-16752 and CMS97-13997, and by ARPA under Grant DABT 63-92-C-0032. The first author acknowledges fruitful discussions with Professor Greg Rodin.

References

Abdel-Tawab, K. and Rodin, G. (1997). *MSS&M Report 97/12*, Research Center for Mechanics of Solids Structures & Materials, The University of Texas at Austin.

Anderson, T.L. (1995). *Fracture Mechanics Fundamentals and Applications*, 2nd Edition, CRC Press.

Azhdari, A. and Nemat-Nasser, S. (1996). *Journal of Mechanics and Physics of Solids* **44**, 929–951.

Azhdari, A. and Nemat-Nasser, S. (1998). To appear in *Mechanics of Materials*.

Ballarini, R., Charalambides, P.G. and Islam, S. (1995). *International Journal of Fracture* **70**, 275–304.

Ballarini, R., Mullen, R.L., Yin, Y., Kahn, H., Stemmer, S. and Heuer, A.H. (1997). *Journal of Materials Research* **12**, 915–922.

Barsoum, R.S. (1977). *International Journal of Numerical Methods in Engineering* **11**, 85.

Bazant, Z.P. (1993). *ASCE Journal of Engineering Mechanics* **119**, 1828–1844.

Carpinteri, A. (1994). *Mechanics of Materials* **18**, 89–101.

Carpinteri, A. and Scavia, C. (1991). In *Fracture Processes in Concrete, Rock and Ceramics*, (Edited by J.G.M. van Mier, J.G. Rots and A. Bakker), E.& F.N. Spon, London, 173–182.

Cox, B.N. and Marshall, D.B. (1994). *Acta Metallurgica et Materialia* **42**, 341–363.

Frost, H.J. and Ashby, M.F. (1982). *Deformation Mechanism Maps*, Pergamon Press, Oxford.

Hutchinson, J.W. (1968). *Journal of the Mechanics and Physics of Solids* **16**, 13–31.

Ingraffea, A.R. and Manu, C. (1980). *International Journal of Numerical Methods in Engineering* **15**, 1427–1445.

Jha, M. (1997). *Ph.D. Dissertation*, Department of Mechanical Engineering, University of Maryland at Baltimore County.

Jha, M., Charalambides, P.G. and Ballarini, R. (1997). *International Journal of Solids and Structures* **34**, 1849–1871.

Kumar, S. (1992). *Ph.D. Dissertation*, Department of Engineering Science and Mechanics, Pennsylvania State University.

Mullen, R.L., Ballarini, R., Yin, Y. and Heuer, A.H. (1997). *Acta Materialia* **45**, 2247–2255.

Rice, J.R. and Rosengren, G.F. (1968). *Journal of the Mechanics and Physics of Solids* **16**, 1–12.

Sih, G.C., Paris, P.C. and Irwin, G.R. (1965). *International Journal of Fracture Mechanics* **1**, 189–203.